Visualization of dynein-dependent microtubule gliding at the cell cortex: implications for spindle positioning

Eva M. Gusnowski and Martin Srayko

Department of Biological Sciences, University of Alberta, Edmonton, Alberta T6G 2E9, Canada

Dynein motors move along the microtubule (MT) lattice in a processive "walking" manner. In the one-cell *Caenorhabditis elegans* embryo, dynein is required for spindle-pulling forces during mitosis. Posteriorly directed spindle-pulling forces are higher than anteriorly directed forces, and this imbalance results in posterior spindle displacement during anaphase and an asymmetric division. To address how dynein could be asymmetrically activated to achieve posterior spindle displacement, we developed an assay to measure dynein's activity on individual MTs at the embryo cortex. Our study reveals that cortical dynein motors maintain a basal level of activity that propels MTs along the cortex, even under experimental conditions that drastically reduce anaphase spindle forces. This suggests that dynein-based MT gliding is not sufficient for anaphase spindle-pulling force. Instead, we find that this form of dynein activity is most prominent during spindle centering in early prophase. We propose a model whereby different dynein–MT interactions are used for specific spindle-positioning tasks in the one-cell embryo.

Introduction

Most multicellular organisms use asymmetric cell division to generate cellular diversity. In *Caenorhabditis elegans*, the first cell division results in two daughters that are developmentally distinct and unequal in size. The size asymmetry is caused by precise positioning of the mitotic spindle toward the posterior of the cell. The spindle-pulling forces require the motor protein dynein and heterotrimeric G protein signaling. Interestingly, many of the factors implicated in asymmetric force generation (e.g., Gα, Gβ, and dynein) are not obviously asymmetrically distributed (Gönczy et al., 1999; Gotta and Ahringer, 2001; Grill et al., 2001; Gotta et al., 2003; Srinivasan et al., 2003). In an effort to understand how asymmetric forces are generated, we developed a method to specifically measure processive dynein motor activity.

In yeast cells, microtubules (MTs) slide along the cortex in a dynein-dependent manner (Adames and Cooper, 2000). Therefore, we sought to quantify similar MT movements at the *C. elegans* cortex. In contrast to the simple MT arrays in yeast cells, *C. elegans* asters contain thousands of MTs that obscure the movements of individual polymers. To better resolve MT movements, we used a GFP-tagged EB1-like EBP-2 (end-binding protein-2; Srayko et al., 2005; Kozlowski et al., 2007) to develop an EB1 velocity assay (EVA). Because EB1 binds to the plus ends of growing MTs, the velocity of EB1 dots relative to the MT minus end represents the growth rate of an individual MT polymer. Furthermore, if the MT moves because of an external force, the EB1 particle will move with a velocity equal to the MT growth rate plus or minus the velocity caused by the external force. A previous study has shown that MT growth rates in the one-cell *C. elegans* embryo are consistent and reproducible between different samples in the same cell cycle stage and throughout the cytoplasm (Srayko et al., 2005). Therefore, we reasoned it should be possible to track EB1 to study the effects of dynein on MT gliding movements at the inner embryonic cortex.

Results and discussion

A population of dynein motors at the embryonic cortex propels MTs during anaphase

Most MTs that contact the cortex grow from centrosomes, where they are anchored at their minus ends and would not be

Correspondence to Martin Srayko: martin.srayko@ualberta.ca

Abbreviations used in this paper: ddMTV, dynein-dependent MT velocity; DIC, differential interference contrast; EVA, EB1 velocity assay; MT, microtubule; NEB, nuclear envelope breakdown.

The Rockefeller University Press $30.00
J. Cell Biol. Vol. 194 No. 3 377–386
www.jcb.org/cgi/doi/10.1083/jcb.201103128

expected to dislodge if pulled on by a motor. In a wild-type embryo, most MTs rapidly depolymerize (~1.4 s) after touching the cortex and do not grow or slide along the cortical surface (Kozlowski et al., 2007). Correspondingly, an important feature of EVA involves the creation of free, unanchored MTs that continue to grow and can slide along the cortex in response to external forces. We released MTs from the centrosome using a temperature-sensitive allele of *mei-1* katanin, *mei-1(ct46)*. MEI-1 is normally female meiosis specific, but the *ct46* mutation causes katanin to persist into the first mitotic division in which it concentrates at centrosomes and chromatin, ectopically severing MTs (Fig. 1 A; Clandinin and Mains, 1993; Clark-Maguire and Mains, 1994; Srayko et al., 2000). Indeed, *mei-1(ct46)* embryos exhibited many EB1 particles moving along the cortex (Video 1), indicating that MT plus ends that approach the cortex at shallow angles do not readily depolymerize. Thus, ectopic MT severing facilitated the tracking of EB1 particles along the inner embryonic cortex and allowed the detection of motor-dependent MT movements (Fig. 1, A and B). Additionally, because dynein motor activity is affected by applied load (Mallik et al., 2004), the katanin-generated free MTs allowed a direct comparison of cortical dynein motor activity under similar light-load conditions.

Dynein motors can exhibit varying walking speeds in vitro (Mallik et al., 2004), which raised the possibility that different areas of the one-cell cortex could modulate dynein speed to achieve asymmetric spindle-pulling forces. However, laser-based centrosome disintegration experiments suggested individual motor speeds need not be different between anterior and posterior cortices, and only the net force applied to the spindle poles appears to be asymmetric (Grill et al., 2003). As such, a higher number of force generators are predicted to be active at the posterior cortex (Grill et al., 2003). Using EVA, we sought to determine whether anterior–posterior asymmetry of force correlates with (a) differences in mean motor-dependent MT gliding velocity or (b) differences in the proportion of cortical MTs that exhibit dynein-dependent gliding.

We assayed embryos in late metaphase/anaphase because pulling forces are active at this time (Grill et al., 2001; Labbé et al., 2004; McCarthy Campbell et al., 2009). To measure EB1 movements caused by MT polymerization alone, we first measured the velocities of EB1 dots moving in a straight line away from the centrosome in the midplane of the embryo. We determined that <2% of EB1 dots emanating from the centrosomes (i.e., anchored MTs) exceeded 1.0 µm/s in control (empty vector) RNAi embryos (Fig. S1). Additionally, previous work showed dynein on the nuclear envelope can propel EB1 to speeds >1.0 µm/s (Srayko et al., 2005). Therefore, to find dynein-dependent MT movements, we focused on EB1 speeds >1.0 µm/s.

We next measured EB1 velocities at the cortex of embryos subjected to either control RNAi treatment or *dhc-1(RNAi)* to reduce dynein heavy chain. We noted a clear decrease in the number of EB1 velocities >1.0 µm/s in *dhc-1(RNAi)* embryos (Fig. 1, C and D; and Video 2). To quantify the proportion of the high-speed population, we used a clustering algorithm to find a nested Gaussian subpopulation having a mean >1.0 µm/s within the total population of EB1 velocities (Materials and methods). In the control, a subpopulation representing 10.7% (110/1,030) of the total EB1 velocities was detected (mean velocity = 1.14 µm/s; Fig. 1 C, dotted line). In *dhc-1(RNAi)* embryos, a subpopulation >1.0 µm/s could not be detected within the search parameters. A few EB1 velocities >1.0 µm/s were present, which we estimated to maximally represent 1.9% (12/642) of the total velocity population (Materials and methods; Fig. 1 D and Video 2). This significant reduction indicated that DHC-1 is required for almost all EB1 velocities >1.0 µm/s at the inner cortex of control embryos ($P = 8.7E-9$; $\alpha = 0.01$). We refer to the fast EB1 speeds as dynein-dependent MT velocities (ddMTVs). We also tested *efa-6*, a gene implicated in depolymerizing MTs at the cortex (O'Rourke et al., 2010). We found that, like ectopic katanin, more EB1 dots moved along the cortex in an *efa-6(ok3533)* background. Unlike ectopic katanin, only a few dots moved faster than 1 µm/s, indicating *efa-6(ok3533)* causes more MTs to grow along the cortex, but the majority of these are still likely attached to the centrosome (Fig. S2; O'Rourke et al., 2010).

lin-5(RNAi) decreases the number of ddMTVs at the inner cortex

EVA detected EB1 movements at the inner cortex, but it is formally possible that long MTs with only their plus ends touching the cortex could be propelled by motor proteins located in subcortical regions of the cytoplasm. To confirm that cortically located dynein is required for the ddMTVs in EVA, we depleted LIN-5. LIN-5 localizes dynein to the inner cortex and is also required for anaphase pulling forces (Srinivasan et al., 2003; Afshar et al., 2005; Nguyen-Ngoc et al., 2007). However, LIN-5 does not interfere with most other postmeiotic dynein-dependent processes that occur deeper in the cytoplasm, such as mitotic spindle assembly (Video 3; van der Voet et al., 2009). Therefore, we tested *lin-5(RNAi)* embryos to determine whether cortical ddMTVs were affected. *lin-5(RNAi)* significantly reduced the proportion of ddMTVs (Fig. 2 A). The clustering algorithm was unable to identify a subpopulation >1.0 µm/s in the *lin-5(RNAi)* dataset. However, a small number of ddMTVs were present above our cutoff value, which we estimated to represent 2.9% maximally (20/679; see Materials and methods), resulting in a significant decrease compared with control values ($P = 3.5E-9$; $\alpha = 0.01$; Fig. 3 A). In agreement with previous work (Nguyen-Ngoc et al., 2007), our data are consistent with LIN-5 linking dynein to the cortex. This result also confirmed that EVA detects cortical ddMTVs specifically.

An anterior-like cortex has more ddMTVs than a posterior-like cortex

We next determined whether there were any differences in ddMTVs at the posterior versus anterior cortices. Because MTs at the cortex could conceivably span both the anterior and posterior domains in a wild-type embryo, we simplified our analysis by generating either an anterior- or posterior-like cortex on a whole embryo scale (via *par-2(RNAi)* or *par-3(RNAi)*, respectively). Previous work showed that anaphase pulling forces on both spindle poles are anterior-like in *par-2(RNAi)* and

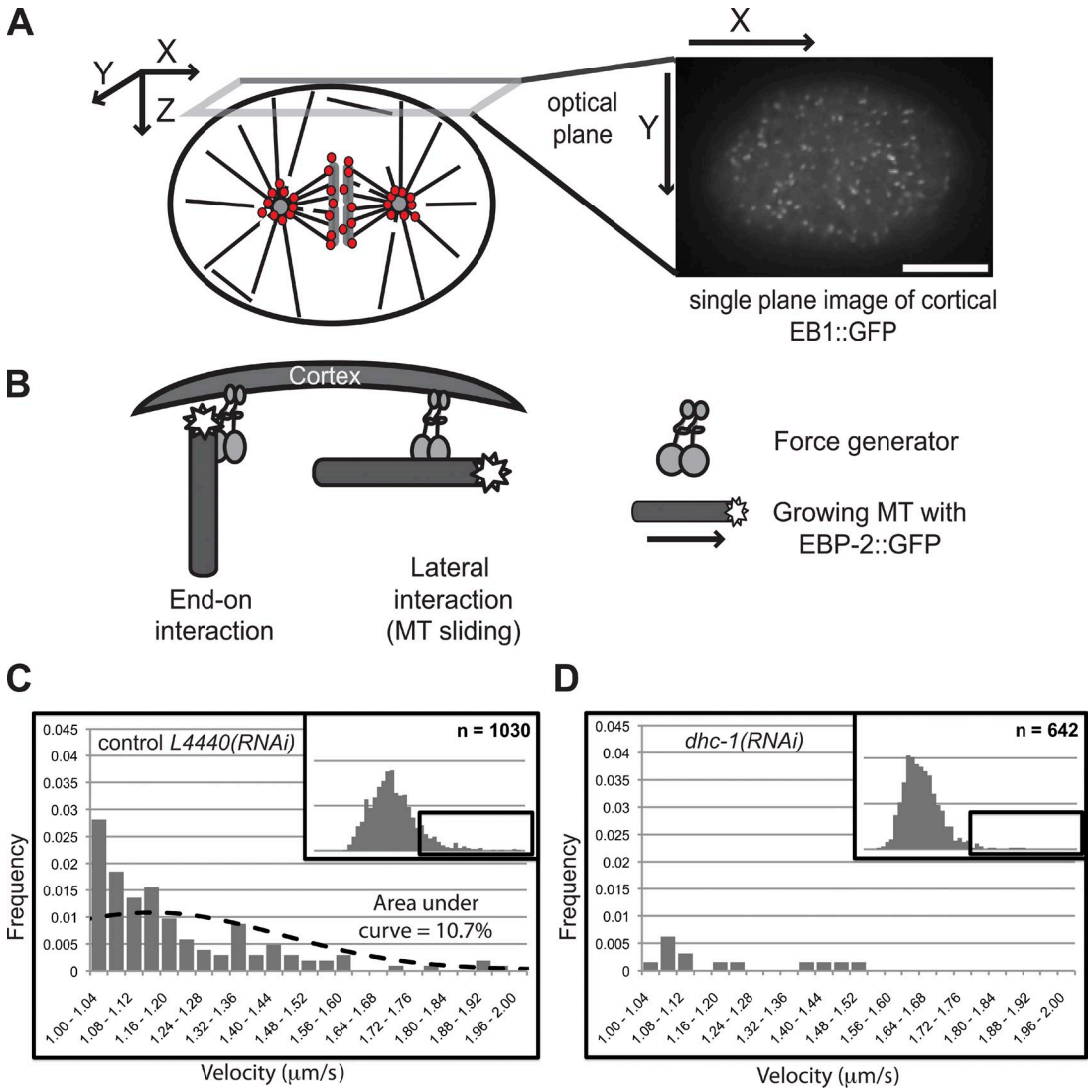

Figure 1. **EVA reveals a dynein-dependent EB1 velocity population at the cortex.** (A) EB1 particles are tracked at the cortex of embryos ectopically expressing the MT-severing enzyme MEI-1 (red circles). Bar, 10 µm. (B) MTs conceivably interact with cortical force generators in an end-on or lateral manner. (C and D) The distribution of EB1 velocities >1.0 µm/s in control *L4440(RNAi) mei-1(ct46)* and *dhc-1(RNAi) mei-1(ct46)* embryos. The insets are the entire velocity distribution; the boxed areas within the inset are enlarged. The dotted line is the computationally derived Gaussian population with a mean >1.0 µm/s. *n* = number of cortical EB1 trajectories. Histograms and population analysis used pooled data (four embryos from one *L4440(RNAi)* trial; 14 embryos from three *dhc-1(RNAi)* trials).

posterior-like in *par-3(RNAi)* (Grill et al., 2001). We expected that ddMTVs in the *par-2(RNAi)* would be significantly decreased. However, we observed a significant increase in the number of ddMTVs at the *par-2(RNAi)* anteriorized cortex compared with control values (20.6%, 190/925; P = 1.7E−9; α = 0.01; Figs. 2 B and 3 A). Furthermore, we did not detect a significant increase in the number of ddMTVs in the *par-3(RNAi)* posteriorized cortex compared with control values (13.90%, 100/716; P = 0.043; α = 0.01; Figs. 2 C and 3 A). Surprisingly, these results indicated that proportionately more dynein motors were active in the anterior (where spindle-pulling forces are weaker) than in the posterior (where spindle-pulling forces are higher). In light of this result, we next tested components of the heterotrimeric G protein pathway for their effect on ddMTVs.

Modulation of heterotrimeric G protein signaling does not significantly change the proportion of ddMTVs

Members of the heterotrimeric G protein pathway regulate cortical force generation and are implicated in the activation of dynein motors at the cortex. Simultaneous depletion of two Gα subunits (GOA-1 and GPA-16; Gα) or the G protein activators GPR-1 and GPR-2 (hereafter referred to as GPR-1/2) severely reduce the rate and extent of anaphase spindle pole separation (Video 4; Colombo et al., 2003; Nguyen-Ngoc et al., 2007). Therefore, the proportion of ddMTVs was expected to decrease significantly when these factors were eliminated. However, we found no significant reduction in the proportion of ddMTVs upon RNAi of *Gα* (9.73%, 66/681; P = 0.58), *gpr-1/2* (10.96%, 62/568; P = 0.87), or *lis-1*, a dynein accessory protein implicated

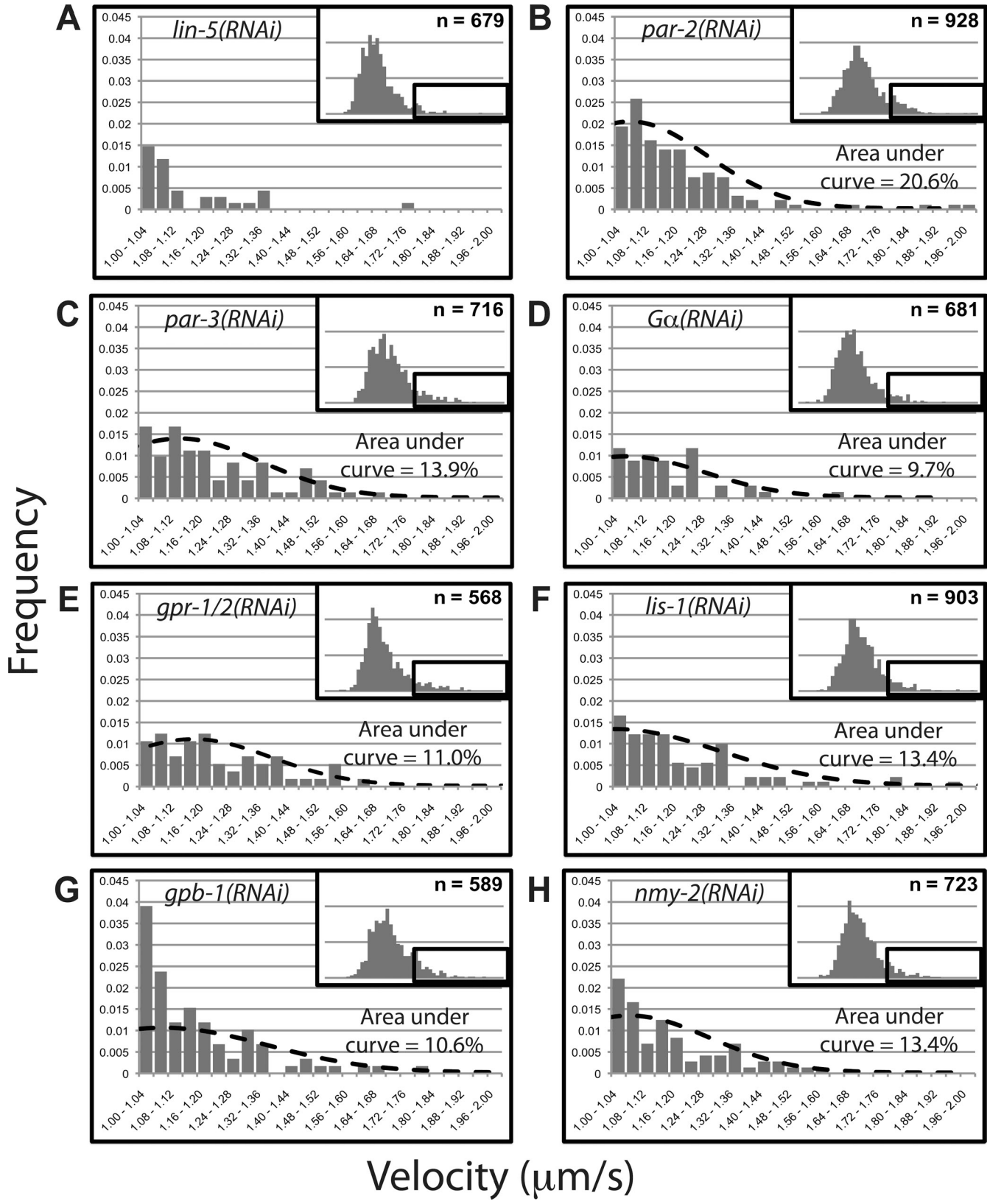

Figure 2. **EVA analysis in various RNAi treatments.** (A–H) The distribution of EB1 velocities >1.0 µm/s in RNAi-treated *mei-1(ct46)* embryos. The insets are the entire velocity distribution; the boxed areas within the insets are enlarged. The dotted lines are the computationally derived Gaussian population with a mean >1.0 µm/s. *n* = number of cortical EB1 trajectories. Each histogram and population analysis used pooled data (at least five embryos from at least two independent RNAi trials).

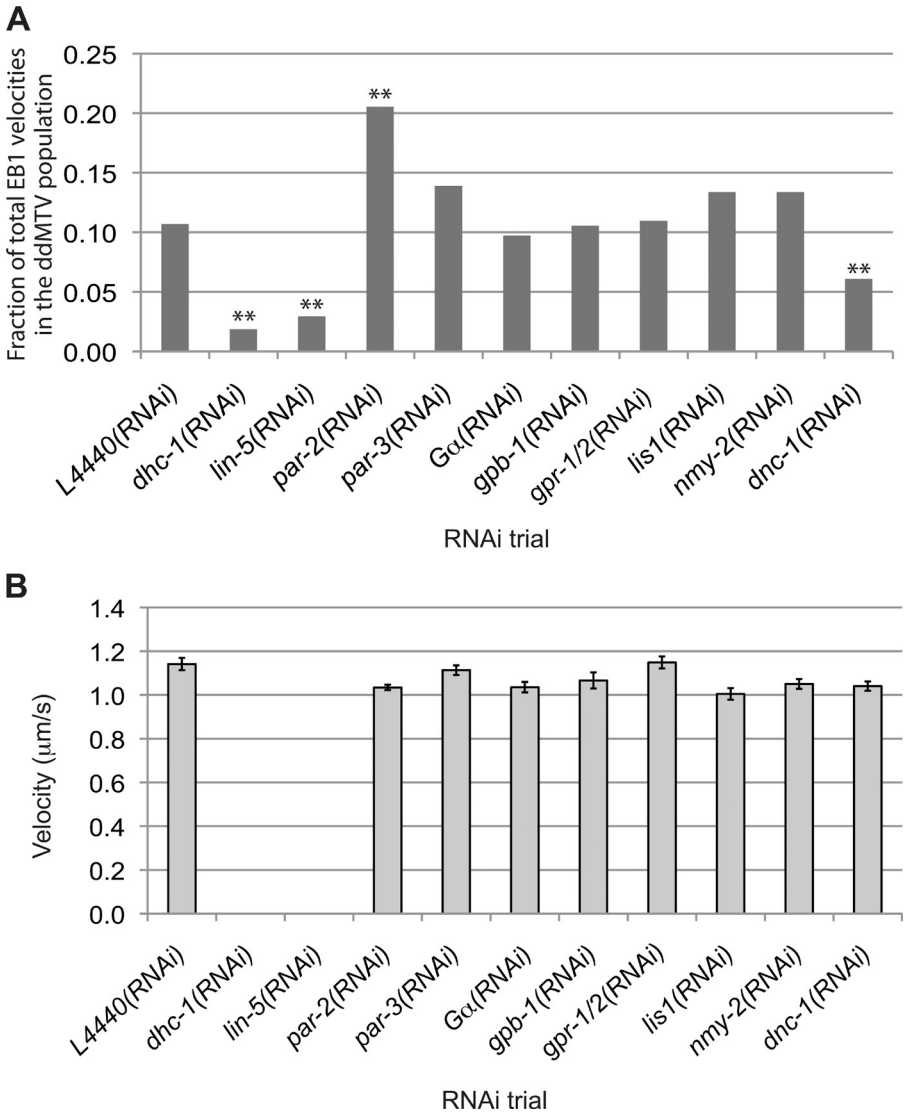

Figure 3. **Relative proportions and mean velocities of the cortical ddMTV populations.** (A) The proportion of EB1 velocities in the ddMTV population are shown. All RNAi was performed in a *mei-1(ct46)* background. *dhc-1(RNAi)* and *lin-5(RNAi)* subpopulations >1.0 μm/s were not detected by the computer algorithm and were estimated (Materials and methods). (B) Mean velocity of the ddMTV subpopulation in micrometers per second. For *dhc-1(RNAi)* and *lin-5(RNAi)*, the mean velocity was not measurable (Materials and methods). Error bars represent SEM. *par-2(RNAi)*, P = 6.5E−4; *par-3(RNAi)*, P = 0.44; *goa-1/gpa-16(RNAi)*, P = 4.6E−3; *gpb-1(RNAi)*, P = 0.11; *gpr-1/2(RNAi)*, P = 0.85; *lis-1(RNAi)*, P = 5.0E−4; *nmy-2(RNAi)*, P = 0.012; *dnc-1(RNAi)*, P = 1.5E−4). The double asterisks indicate significance at α = 0.01. Population analysis used pooled data (at least four embryos from at least two independent RNAi trials, except *L4440(RNAi)* and *dnc-1(RNAi)*, which were from one RNAi trial).

in cortically located anaphase spindle-pulling forces (13.38%, 120/903; P = 0.070 at α = 0.01; Figs. 2, D–F, and 3 A; Videos 5, 6, and 7; Cockell et al., 2004). The *lis-1(RNAi)* result was surprising because LIS-1 is required for a wide variety of dynein-dependent processes (Cockell et al., 2004). However, LIS-1 is implicated in affecting dynein motor activity under high load (McKenney et al., 2010), and EVA measures motor activity under low load, which might explain why no decrease in ddMTV proportion was observed in *lis-1(RNAi)* embryos. We next tested whether ectopic activation of G protein signaling would increase the proportion of ddMTVs. *gpb-1(RNAi)* embryos have reduced Gβ levels and exhibit an overall increase in cortical pulling forces during anaphase (Video 4; Gotta and Ahringer, 2001; Afshar et al., 2005). However, *gpb-1(RNAi)* did not increase the proportion of ddMTVs compared with control values (10.55%, 62/589; P = 0.93; α = 0.01; Figs. 2 G and 3 A and Video 8).

To test whether cortical contractility affects ddMTVs, we depleted the nonmuscle myosin NMY-2. NMY-2 is required for polarity establishment and force generation in the embryo (Cuenca et al., 2003; Munro et al., 2004), possibly through the modulation of the elasticity of underlying substrates to which force generators like dynein could be linked (Kozlowski et al., 2007). As with the G protein activators, RNAi of *nmy-2* also failed to significantly alter the proportion of ddMTVs compared with control values (13.38%, 97/723; P = 0.087; α = 0.01; Figs. 2 H and 3 A and Video 9).

Our data also allowed a comparison of the mean speed of the ddMTVs in the various RNAi trials. We found that the *par-2(RNAi)*, *Gα(RNAi)*, and *lis-1(RNAi)* embryos exhibited slight differences in mean ddMTVs compared with the control RNAi dataset (Fig. 3 B). However, there was no consistent trend to indicate that individual motors propel MTs faster when activated by the G protein pathway.

A large volume of work suggests Gα, GPR-1/2, LIN-5, and LIS-1 likely form a complex required for dynein-dependent spindle-pulling forces (Gotta and Ahringer, 2001; Gotta et al., 2003; Srinivasan et al., 2003; Afshar et al., 2004, 2005; Cockell et al., 2004; Couwenbergs et al., 2007; Nguyen-Ngoc et al., 2007; Park and Rose, 2008). Our experiments demonstrate a potential separation of function for dynein motor activity at the cortex: clearly, it is possible to eliminate most of the anaphase

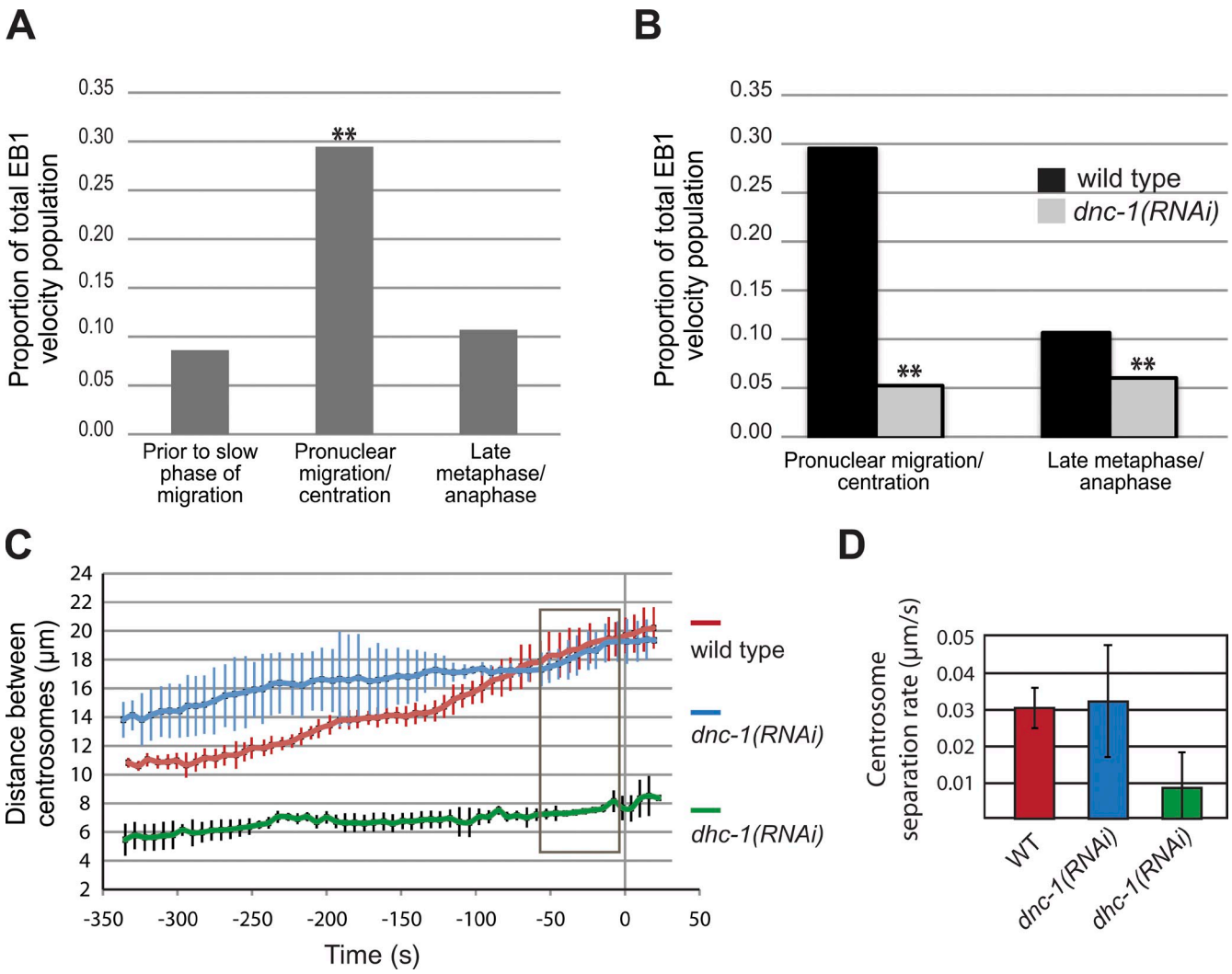

Figure 4. ***dnc-1(RNAi)* reduces cortical MT gliding but not centrosome separation.** (A) Cortical ddMTV proportions throughout the wild-type (WT) cell cycle. In the one-cell embryo, the proportion of ddMTVs increased during pronuclear migration/centration compared with anaphase (29.5%, 69/234; P = 2.1E−6). *mei-1(ct46)* embryos were used for pronuclear migration/centration and slow phase stages. *L4440(RNAi) mei-1(ct46)* embryos from Fig. 1 C were used for anaphase. (B) *dnc-1(RNAi)* reduces the proportion of ddMTVs during pronuclear migration/centration (5.3%, 21/397; P = 3.2E−4) and anaphase (6.1%, 63/1,040; P = 1.5E−4) compared with control. Significance at $\alpha = 0.01$ in A and B is indicated by double asterisks. Data in A and B were derived from at least four embryos pooled before population analysis from single RNAi trials (except pronuclear migration/centration *dnc-1(RNAi)* from two independent RNAi trials). (C) Both *dnc-1(RNAi)* and *dhc-1(RNAi)* embryos exhibit defects in centration (Video 10), but only *dhc-1(RNAi)* significantly reduced centrosome separation rates in anaphase. The box represents 53 ± 2 s before cytokinesis furrow ingression (t = 0). *n* = 4 embryos. (D) Mean rates of centrosome separation for the interval boxed in C are shown. SEM at 95% confidence is shown.

pulling forces on the mitotic spindle while still maintaining a population of active cortical motors. Even though cortical dynein is capable of exerting force on individual MTs through lattice interactions, this behavior alone is not sufficient for the spindle-pulling force in anaphase.

To understand the potential function of MT gliding, we noted that ddMTVs were most abundant during pronuclear migration and centrosome/nuclear centration, before metaphase (29.5%, 69/235; Fig. 4 A). LIN-5, the only component other than dynein found to reduce ddMTVs, is also required for efficient pronuclear/centrosome centering (Park and Rose, 2008). Therefore, we predicted that any genes required for pronuclear/centrosome centering, but not anaphase, should perturb ddMTVs without affecting anaphase force. We tested dynactin, a protein implicated in increasing dynein motor processivity along the MT lattice (King and Schroer, 2000). In worm embryos, *dnc-1(RNAi)* causes pronuclear/centrosomal complex centration defects but centrosomes still separate around the male pronucleus, suggesting that some dynein-dependent processes are still functional (23/23 embryos, this study; Skop and White, 1998; O'Rourke et al., 2011). Furthermore, we found ddMTVs were significantly reduced in *dnc-1(RNAi)* during anaphase (10.7 vs. 6.1%; P = 1.5E−4) as well as pronuclear migration/centration (29.5 vs. 5.3%; P = 3.2E−4; Fig. 4 B) at $\alpha = 0.01$. Despite the observed centration defects, *dnc-1(RNAi)* embryos exhibited relatively dynamic centrosome movement during anaphase, with centrosomes separating just before cytokinesis at rates similar to control RNAi (Fig. 4, C and D; and Video 10). We conclude that dynactin is required for robust MT gliding at the cortex, and this behavior contributes to pronuclear/centrosome centering.

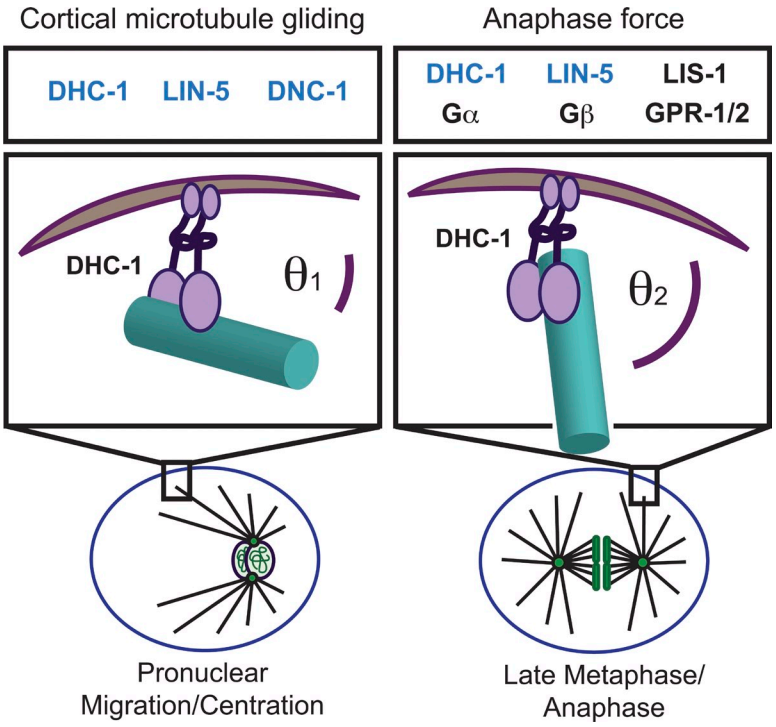

Figure 5. **A model for two functionally distinct populations of dynein at the embryo cortex.** DHC-1, LIN-5, and DNC-1 are necessary for MT gliding behavior and generate force by pulling on MTs that contact the cortex at shallow angles (θ1), contributing to pronuclear centration (left; blue text). DHC-1, LIN-5, and members of the heterotrimeric G protein pathway are necessary for normal anaphase spindle-pulling forces (right), but many of these components did not significantly alter MT gliding behavior (black text). Because most MTs contact the cortex at orthogonal angles in the one-cell metaphase/anaphase embryo (θ2), anaphase force likely occurs primarily through end-on interactions (right). The two mechanisms proposed are shown to reflect relative contributions and are not necessarily mutually exclusive.

Two distinct mechanisms of dynein-dependent force generation at the cortex

Based on our results, we suggest there are at least two distinct mechanisms of dynein-dependent force generation at the cortex: one that moves MTs only through motor–lattice interactions (and is responsible for ddMTVs in EVA), and a second that generates spindle-pulling forces through a mechanism that does not use processive MT motor "walking" activity alone. In budding yeast cells, spindle positioning utilizes both lateral and end-on MT interactions with cortical force generators (Carminati and Stearns, 1997; Adames and Cooper, 2000). Interestingly, end-on MT interactions seem to be strongly correlated with spindle displacement (Carminati and Stearns, 1997). As in yeast, our data suggest two mechanistically distinct modes of MT pulling in *C. elegans*.

Because MTs predominantly polymerize from the centrosomes, it is likely that cortically located force generators interact with MT plus ends (Gönczy, 2002; Grill et al., 2003). Although it is difficult to detect MT end-on interactions in the *C. elegans* embryo, one study revealed the existence of cortical invaginations at the embryonic cortex during anaphase (Redemann et al., 2010). These invaginations are dependent on dynein and members of the G protein pathway and probably represent a major contribution to spindle-pulling forces in anaphase. However, MT gliding could contribute to residual spindle movements by pulling on MTs that contact the cortex at shallow angles. Our observations suggest that these MTs are rare in wild-type anaphase (because of geometrical constraints) but abundant during the first embryonic prophase when the pronuclear/centrosomal complex migrates to the center. We postulate that cortical MT gliding and end-on interactions as well as cytoplasmic pulling forces (Kimura and Kimura, 2011) could each contribute to centrosome/pronuclear centering.

The two modes of dynein–MT interactions proposed in Fig. 5 are probably not used exclusively, but rather, their relative proportions could be altered to regulate pulling force. Because GPR-1/2 is present at a higher level at the posterior cortex during metaphase/anaphase and is required for force asymmetry (Colombo et al., 2003; Gotta et al., 2003; Tsou et al., 2003), this could be a key factor that determines the different modes of MT pulling at the cortex. In specifying cortical polarity, the partitioning-defective proteins could also determine which pulling mechanism is used (i.e., via GPR-1/2 localization; Colombo et al., 2003; Gotta et al., 2003; Tsou et al., 2003). In this way, *par-2(RNAi)* would be expected to shift the balance away from MT end interactions to more lateral MT interactions, explaining our observed increase in the number of ddMTVs in these embryos.

In conclusion, we have shown that cortical dynein-dependent MT gliding behavior is not sufficient to generate significant pulling forces during anaphase in the one-cell embryo; rather, it is implicated in generating forces to help center the spindle in prophase. Our results fit well with computer simulations that suggest force generation by dynein motor activity along the MT lattice alone is probably insufficient to explain the level of forces observed during metaphase and anaphase in vivo (Kozlowski et al., 2007). Instead, the ability of a cortically localized factor to hold on to a depolymerizing MT could provide sufficient levels of force (Grishchuk et al., 2005). In support of this idea, normal MT dynamics are required for force generation and asymmetric spindle positioning in the embryo (Nguyen-Ngoc et al., 2007). Therefore, we suggest that the modulators of anaphase forces do not turn dynein motor activity on/off, per se, but rather, they might facilitate end-on interactions between MTs and dynein.

Materials and methods

RNAi by feeding

RNAi plates (nematode growth medium agar, 1.0 mM IPTG, and 25 mg/ml carbenicillin) were seeded with the desired RNAi feeding clone and cultured overnight at RT to express double-stranded RNA. Control RNAi was the L4440 RNAi feeding vector (Addgene, Inc.; A. Fire, Stanford University School of Medicine, Stanford, CA) lacking an insert. RNAi feeding clones used in this study are previously described in Kamath et al. (2003) with the exception of *gpa-16*, which was cloned using the primers 5′-GCCCCGGGTGCTCAAAGAAGACGGC-3′ and 5′-AAACTAGTTTCCCGAATCGGACCAAA-3′. *mei-1(ct46)* worms were provided by P. Mains (University of Calgary, Calgary, Alberta, Canada).

MAS94 (*unc-119(ed3)abcIs3[pie-1-ebp-2–gfp;unc-119(+)]; mei-1(ct46)unc-13(e1091)*) L4 *C. elegans* larvae were cultured on the RNAi plates at 25°C for ≥17 h (*dhc-1(RNAi)*, *par-2(RNAi)*, and *par-3(RNAi)*), ≥24 h (*L4440(RNAi)*, *gpr-2(RNAi)*, *gpb-1(RNAi)*, *lin-5(RNAi)*, *lis-1(RNAi)*, and *nmy-2(RNAi)*), or ≥25 h (*dnc-1(RNAi)*). *gpr-2(RNAi)* was used to knock out both GPR-1 and GPR-2, as these proteins are 96% identical at the nucleotide level (Srinivasan et al., 2003). In the case of *goa-1(RNAi)/gpa-16(RNAi)*, a 1:1 mixture of the two cultures was seeded onto RNAi plates. MAS94 L4 hermaphrodites were left for ≥36 h on the *Gα(RNAi)* plates. Some genes exhibited phenotypes that were recognizable in the *mei-1(ct46)* background (*mei-1(ct46)* causes a mispositioned mitotic spindle), allowing a direct assessment of the effectiveness of the RNAi treatment (*dhc-1(RNAi)*, *lin-5(RNAi)*, *lis-1(RNAi)*, and *nmy-2(RNAi)*). RNAi depletion was also confirmed for all other genes by differential interference contrast (DIC) microscopy of parallel-fed EB1-GFP worms (MAS37, genotype: *unc-119(ed3)abcIs3[pie-1-ebp-2–gfp;unc-119(+)]*; Video 4) or transgenic worms expressing fluorescent markers PAR-2–GFP and PAR-6–mCherry (MAS1, genotype: *itIs153; ddIs26 [par-2–gfp; rol-6(su1006); par-6-mCherry; unc-119(+)]*; Fig. S3 A). For *gpr-1/2(RNAi)*, the anaphase phenotype was not always obviously symmetric, which is consistent with previous studies (Colombo et al., 2003; Tsou et al., 2003). Therefore, GPR-1/2 protein levels were directly assayed via Western blotting performed on embryonic lysates from a cohort of *gpr-2(RNAi)* worms used in parallel for EVA (Fig. S3 B). RB2543 L4 hermaphrodites that contain a deletion in the *efa-6* gene (genotype: *efa-6(ok3533)* IV; created by the *C. elegans* Gene Knockout Consortium; provided by the Caenorhabditis Genetics Center) were incubated for ≥24 h on *mel-26(RNAi)* plates.

Imaging and temperature control protocol

Worms used for ex utero imaging were dissected in 340 mOsm egg buffer (188 mM NaCl, 48 mM KCl, 2 mM $CaCl_2$, 2 mM $MgCl_2$, and 25 mM Hepes, pH 7.3) and mounted on a thin 2% agarose pad. Imaging was performed with an inverted microscope (IX81; Olympus; 60×, NA 1.42 oil objective) with a spinning-disc confocal head (CSU10; Yokogawa) modified with a condenser lens in the optical path (Quorum Technologies). All imaging was performed with a camera (ORCA-R2; Hamamatsu Photonics) controlled by MetaMorph software (Molecular Devices). The imaging environment temperature was controlled with a water circulator (Haake) pumping through a collar on the objective. The temperature of the immersion oil on the coverslip was recorded immediately after the final image of each embryo and was maintained at 20 ± 0.5°C.

EB1 velocities were obtained during metaphase and anaphase. Before GFP acquisition, a DIC time-lapse video was recorded at the pronuclear/centrosomal focal plane to discern the point of nuclear envelope breakdown (NEB). During late metaphase/anaphase the focal plane was moved to the cell cortex and defined as the plane where yolk granules are first detected below the eggshell. This method was confirmed via the use of the cortical marker PAR-2–GFP, in which GFP images were taken to determine the relationship between the DIC image and the cortex (unpublished data). The GFP images were acquired every 300 ms (stream acquisition with no binning to maximize pixel resolution). After 300 GFP images, another DIC image was captured, and the focal plane returned to the centrosomes. Because anaphase takes ∼90 s to complete and cytokinesis occurs ∼1–2 min after anaphase (Cowan and Hyman, 2004; Oegema and Hyman, 2006), only embryos that formed a cytokinetic furrow within 2 min of the end of the GFP stream acquisition were used for EVA tracking. This controlled for cell cycle delays that might result from RNAi treatment. For *nmy-2(RNAi)* embryos, which fail to generate a cytokinetic furrow, we empirically determined the mean time between NEB and anaphase onset in a cohort of RNAi embryos (n = 3) and, thus, initiated GFP acquisition 4 min and 31 s after NEB.

Tracking EB1-GFP and centrosomes

ImageJ (National Institutes of Health) was used to track the movement of EB1 points, using the ImageJ particle detector and tracker program (Sbalzarini and Koumoutsakos, 2005). TIFF image stacks were converted into 8-bit grayscale. Object size was limited to a 3-pixel radius, and the search area was restricted to a 10-pixel radius in the following frame. Threshold values were adjusted to maximize the number of EB1 particles detected in the first frame. The resulting tracks were filtered to show only those present for at least five frames (totaling 1.2 s or greater). All tracks were manually inspected to ensure that a single EB1 particle was followed. Excel 2008 (Microsoft) was used to calculate the velocity and create graphs. For growth rate measurements made in the embryo midplane, centrosomes were tracked manually with ImageJ and subtracted from the EB1 positions to correct for centrosomal movement. Centrosome positions for Fig. 4 were obtained by manually tracking x, y, and z positions using MetaMorph software. TH32 (genotype: *unc-119(ed3) ruIs32 III; ddIs6*) embryos were imaged with a spinning-disc confocal microscope as described in the previous section using z-stack (2-µm spacing; 7-s interval between stacks) or single-plane time-lapse acquisition. The first visible sign of cytokinesis furrow ingression was used as a reference (t = 0).

Statistical analysis

Resulting velocities for each set of RNAi embryos were imported into MATLAB software (MathWorks). Velocity data points from all embryos in a given RNAi trial were pooled before population analysis. The mmvn_toolkit was used to determine the mean velocity, variance, and proportion of normal Gaussian populations in the entire velocity datasets. The mean velocity and variance of the Gaussian populations were found via the mmvn_fit(X,k) function (in which X represents the velocity dataset and k represents the number of normal populations/clusters that the program will search for). To detect a subpopulation having a mean value exceeding 1.0 µm/s, we increased the k value until a population >1.0 µm/s was detected by the clustering algorithm to a maximum of k = 5 subpopulations. In the *dhc-1(RNAi)* and *lin-5(RNAi)* datasets, no recognizable population of velocities was found >1.0 µm/s within the search parameters. Assuming that the remaining high velocity EB1 particles in these two trials have a normal distribution and the same mean ddMTV value as the control RNAi treatment (1.14 µm/s), then the proportion of velocities in this population can be estimated using the following equation: [(bin values > 1.14) × 2] + (bin value of 1.12 − 1.16). ddMTV population proportions were compared via a hypothesis test at α = 0.01 and z critical = ±2.575. Mean velocities of the ddMTV populations were compared with the control *L4440(RNAi)* value via a two-tailed Student's *t* test assuming unequal variances at α = 0.01.

Western blotting

Western blotting was performed to confirm the absence of GPR-1/2 in the *gpr-2(RNAi)* embryos as previously described (Hannak et al., 2002). In brief, MAS94 L4 hermaphrodites were plated with *Escherichia coli* expressing either *gpr-2* or control L4440 double-stranded RNA at 25°C for 24 h. After incubation, 250 worms each from the *gpr-2(RNAi)* and *L4440(RNAi)* trials were picked into tubes with 1 ml M9 buffer (22 mM KH_2PO_4, 42 mM Na_2HPO_4, 85 mM NaCl, and 1 mM $MgSO_4$). Worms were pelleted at 1,000 *g* for 1 min and washed 3× in M9, leaving a final volume of 50 µl. Freshly prepared 2× bleach solution (27.5 µl H_2O, 5 µl of 10-M NaOH, and 17.5 µl NaOCl) was added to each tube and vortexed for 3 min to dissolve the hermaphrodite worms. Embryos were pelleted at 1,000 *g* for 1 min and washed 3× in 400 µl embryo wash buffer (0.1 M Tris, pH 7.5, 100 mM NaCl, and 0.1% Tween 20), leaving a final volume of 10 µl. An equal volume of 2× Laemmli sample buffer (Sigma-Aldrich) was added to each tube, and the embryos were lysed in a water bath sonicator for 10 min at RT followed by boiling at 95°C for 5 min. Samples were loaded into a 10% SDS-PAGE resolving gel. A prestained broad-range protein marker (7–175 kD; New England Biolabs, Inc.) was used to determine the relative mass of the proteins. After electrophoresis, the proteins were transferred to a Hi-bond N nitrocellulose membrane. The membrane was blocked for 48 h (4°C) in TBST (TBS and Tween 20; 20 mM Tris-HCl, pH 7.4, 500 mM NaCl, and 0.05% Tween 20) + 8% skim milk. The GPR-1/2 antibody (a gift from L. Rose, University of California, Davis, Davis, CA) and DM1A α-tubulin antibody were both used at 1:5,000 in TBST + 4% skim milk and incubated for 1 h at RT. Goat anti–rabbit and goat anti–mouse HRP-bound secondary antibodies (Bio-Rad Laboratories) were used at 1:5,000 in TBST + 4% skim milk. Antibody binding was detected via an ECL kit (SuperSignal West Pico; Thermo Fisher Scientific).

Online supplemental material

Fig. S1 shows EB1-GFP velocities from the centrosomes. Fig. S2 shows *efa-6(ok3533)* cortical EB1 measurements. Fig. S3 shows RNAi control treatment analysis. Video 1 shows the effect of katanin-mediated release of MTs from the centrosome. Video 2 shows a representative *dhc-1(RNAi); mei-1(ct46); ebp-2–gfp* one-cell *C. elegans* embryo. Video 3 shows a representative *lin-5(RNAi); mei-1(ct46); ebp-2–gfp* one-cell *C. elegans* embryo. Video 4 shows DIC videos of *ebp-2–gfp C. elegans* embryos to confirm RNAi phenotypes for a parallel-fed cohort of worms used for cortical EB1 measurements. Video 5 shows a representative *goa-1/gpa-16(RNAi); mei-1(ct46); ebp-2–gfp* one-cell *C. elegans* embryo. Video 6 shows a representative *gpr-1/2(RNAi); mei-1(ct46); ebp-2–gfp* one-cell *C. elegans* embryo. Video 7 shows a representative *lis-1(RNAi); mei-1(ct46); ebp-2–gfp* one-cell *C. elegans* embryo. Video 8 shows a representative *gpb-1(RNAi); mei-1(ct46); ebp-2–gfp* one-cell *C. elegans* embryo. Video 9 shows a representative *nmy-2(RNAi); mei-1(ct46); ebp-2–gfp* one-cell *C. elegans* embryo. Video 10 shows centrosome separation in wild-type, *dhc-1(RNAi)*-, or *dnc-1(RNAi)*-treated TH32 *γ-tubulin–gfp; histone-gfp* one-cell embryos. Online supplemental material is available at http://www.jcb.org/cgi/content/full/jcb.201103128/DC1.

We thank Drs. Adriana Dawes and Lesilee Rose for comments on the manuscript.

This work was funded by grants from Canadian Institutes of Health Research (CIHR), Alberta Heritage Foundation for Medical Research (AHFMR), and Alberta Ingenuity (AI). M. Srayko was supported by scholar awards from AHFMR and CIHR, and E.M. Gusnowski was supported by awards from the Natural Sciences and Engineering Research Council and AI.

Submitted: 24 March 2011
Accepted: 5 July 2011

References

Adames, N.R., and J.A. Cooper. 2000. Microtubule interactions with the cell cortex causing nuclear movements in *Saccharomyces cerevisiae*. *J. Cell Biol.* 149:863–874. doi:10.1083/jcb.149.4.863

Afshar, K., F.S. Willard, K. Colombo, C.A. Johnston, C.R. McCudden, D.P. Siderovski, and P. Gönczy. 2004. RIC-8 is required for GPR-1/2-dependent Gα function during asymmetric division of *C. elegans* embryos. *Cell*. 119:219–230. doi:10.1016/j.cell.2004.09.026

Afshar, K., F.S. Willard, K. Colombo, D.P. Siderovski, and P. Gönczy. 2005. Cortical localization of the Gα protein GPA-16 requires RIC-8 function during *C. elegans* asymmetric cell division. *Development*. 132:4449–4459. doi:10.1242/dev.02039

Carminati, J.L., and T. Stearns. 1997. Microtubules orient the mitotic spindle in yeast through dynein-dependent interactions with the cell cortex. *J. Cell Biol.* 138:629–641. doi:10.1083/jcb.138.3.629

Clandinin, T.R., and P.E. Mains. 1993. Genetic studies of *mei-1* gene activity during the transition from meiosis to mitosis in *Caenorhabditis elegans*. *Genetics*. 134:199–210.

Clark-Maguire, S., and P.E. Mains. 1994. Localization of the *mei-1* gene product of *Caenorhaditis elegans*, a meiotic-specific spindle component. *J. Cell Biol.* 126:199–209. doi:10.1083/jcb.126.1.199

Cockell, M.M., K. Baumer, and P. Gönczy. 2004. *lis-1* is required for dynein-dependent cell division processes in *C. elegans* embryos. *J. Cell Sci.* 117:4571–4582. doi:10.1242/jcs.01344

Colombo, K., S.W. Grill, R.J. Kimple, F.S. Willard, D.P. Siderovski, and P. Gönczy. 2003. Translation of polarity cues into asymmetric spindle positioning in *Caenorhabditis elegans* embryos. *Science*. 300:1957–1961. doi:10.1126/science.1084146

Couwenbergs, C., J.C. Labbé, M. Goulding, T. Marty, B. Bowerman, and M. Gotta. 2007. Heterotrimeric G protein signaling functions with dynein to promote spindle positioning in *C. elegans*. *J. Cell Biol.* 179:15–22. doi:10.1083/jcb.200707085

Cowan, C.R., and A.A. Hyman. 2004. Asymmetric cell division in *C. elegans*: cortical polarity and spindle positioning. *Annu. Rev. Cell Dev. Biol.* 20:427–453. doi:10.1146/annurev.cellbio.19.111301.113823

Cuenca, A.A., A. Schetter, D. Aceto, K. Kemphues, and G. Seydoux. 2003. Polarization of the *C. elegans* zygote proceeds via distinct establishment and maintenance phases. *Development*. 130:1255–1265. doi:10.1242/dev.00284

Gönczy, P. 2002. Mechanisms of spindle positioning: focus on flies and worms. *Trends Cell Biol.* 12:332–339. doi:10.1016/S0962-8924(02)02306-1

Gönczy, P., S. Pichler, M. Kirkham, and A.A. Hyman. 1999. Cytoplasmic dynein is required for distinct aspects of MTOC positioning, including centrosome separation, in the one cell stage *Caenorhabditis elegans* embryo. *J. Cell Biol.* 147:135–150. doi:10.1083/jcb.147.1.135

Gotta, M., and J. Ahringer. 2001. Distinct roles for Gα and Gβγ in regulating spindle position and orientation in *Caenorhabditis elegans* embryos. *Nat. Cell Biol.* 3:297–300. doi:10.1038/35060092

Gotta, M., Y. Dong, Y.K. Peterson, S.M. Lanier, and J. Ahringer. 2003. Asymmetrically distributed *C. elegans* homologs of AGS3/PINS control spindle position in the early embryo. *Curr. Biol.* 13:1029–1037. doi:10.1016/S0960-9822(03)00371-3

Grill, S.W., P. Gönczy, E.H.K. Stelzer, and A.A. Hyman. 2001. Polarity controls forces governing asymmetric spindle positioning in the *Caenorhabditis elegans* embryo. *Nature*. 409:630–633. doi:10.1038/35054572

Grill, S.W., J. Howard, E. Schäffer, E.H.K. Stelzer, and A.A. Hyman. 2003. The distribution of active force generators controls mitotic spindle position. *Science*. 301:518–521. doi:10.1126/science.1086560

Grishchuk, E.L., M.I. Molodtsov, F.I. Ataullakhanov, and J.R. McIntosh. 2005. Force production by disassembling microtubules. *Nature*. 438:384–388. doi:10.1038/nature04132

Hannak, E., K. Oegema, M. Kirkham, P. Gönczy, B. Habermann, and A.A. Hyman. 2002. The kinetically dominant assembly pathway for centrosomal asters in *Caenorhabditis elegans* is γ-tubulin dependent. *J. Cell Biol.* 157:591–602. doi:10.1083/jcb.200202047

Kamath, R.S., A.G. Fraser, Y. Dong, G. Poulin, R. Durbin, M. Gotta, A. Kanapin, N. Le Bot, S. Moreno, M. Sohrmann, et al. 2003. Systematic functional analysis of the *Caenorhabditis elegans* genome using RNAi. *Nature*. 421:231–237. doi:10.1038/nature01278

Kimura, K., and A. Kimura. 2011. Intracellular organelles mediate cytoplasmic pulling force for centrosome centration in the *Caenorhabditis elegans* early embryo. *Proc. Natl. Acad. Sci. USA*. 108:137–142. doi:10.1073/pnas.1013275108

King, S.J., and T.A. Schroer. 2000. Dynactin increases the processivity of the cytoplasmic dynein motor. *Nat. Cell Biol.* 2:20–24. doi:10.1038/71338

Kozlowski, C., M. Srayko, and F. Nedelec. 2007. Cortical microtubule contacts position the spindle in *C. elegans* embryos. *Cell*. 129:499–510. doi:10.1016/j.cell.2007.03.027

Labbé, J.-C., E.K. McCarthy, and B. Goldstein. 2004. The forces that position a mitotic spindle asymmetrically are tethered until after the time of spindle assembly. *J. Cell Biol.* 167:245–256. doi:10.1083/jcb.200406008

Mallik, R., B.C. Carter, S.A. Lex, S.J. King, and S.P. Gross. 2004. Cytoplasmic dynein functions as a gear in response to load. *Nature*. 427:649–652. doi:10.1038/nature02293

McCarthy Campbell, E.K., A.D. Werts, and B. Goldstein. 2009. A cell cycle timer for asymmetric spindle positioning. *PLoS Biol.* 7:e1000088. doi:10.1371/journal.pbio.1000088

McKenney, R.J., M. Vershinin, A. Kunwar, R.B. Vallee, and S.P. Gross. 2010. LIS1 and NudE induce a persistent dynein force-producing state. *Cell*. 141:304–314. doi:10.1016/j.cell.2010.02.035

Munro, E., J. Nance, and J.R. Priess. 2004. Cortical flows powered by asymmetrical contraction transport PAR proteins to establish and maintain anterior-posterior polarity in the early *C. elegans* embryo. *Dev. Cell*. 7:413–424. doi:10.1016/j.devcel.2004.08.001

Nguyen-Ngoc, T., K. Afshar, and P. Gönczy. 2007. Coupling of cortical dynein and Gα proteins mediates spindle positioning in *Caenorhabditis elegans*. *Nat. Cell Biol.* 9:1294–1302. doi:10.1038/ncb1649

O'Rourke, S.M., S.N. Christensen, and B. Bowerman. 2010. *Caenorhabditis elegans* EFA-6 limits microtubule growth at the cell cortex. *Nat. Cell Biol.* 12:1235–1241. doi:10.1038/ncb2128

O'Rourke, S.M., C. Carter, L. Carter, S.N. Christensen, M.P. Jones, B. Nash, M.H. Price, D.W. Turnbull, A.R. Garner, D.R. Hamill, et al. 2011. A survey of new temperature-sensitive, embryonic-lethal mutations in *C. elegans*: 24 alleles of thirteen genes. *PLoS ONE*. 6:e16644. doi:10.1371/journal.pone.0016644

Oegema, K., and A.A. Hyman. 2006. Cell division. *WormBook*. 19:1–40. doi:10.1895/wormbook.1.72.1

Park, D.H., and L.S. Rose. 2008. Dynamic localization of LIN-5 and GPR-1/2 to cortical force generation domains during spindle positioning. *Dev. Biol.* 315:42–54. doi:10.1016/j.ydbio.2007.11.037

Redemann, S., J. Pecreaux, N.W. Goehring, K. Khairy, E.H.K. Stelzer, A.A. Hyman, and J. Howard. 2010. Membrane invaginations reveal cortical sites that pull on mitotic spindles in one-cell *C. elegans* embryos. *PLoS ONE*. 5:e12301. doi:10.1371/journal.pone.0012301

Sbalzarini, I.F., and P. Koumoutsakos. 2005. Feature point tracking and trajectory analysis for video imaging in cell biology. *J. Struct. Biol.* 151:182–195. doi:10.1016/j.jsb.2005.06.002

Skop, A.R., and J.G. White. 1998. The dynactin complex is required for cleavage plane specification in early *Caenorhabditis elegans* embryos. *Curr. Biol.* 8:1110–1116. doi:10.1016/S0960-9822(98)70465-8

Srayko, M., D.W. Buster, O.A. Bazirgan, F.J. McNally, and P.E. Mains. 2000. MEI-1/MEI-2 katanin-like microtubule severing activity is required for *Caenorhabditis elegans* meiosis. *Genes Dev.* 14:1072–1084.

Srayko, M., A. Kaya, J. Stamford, and A.A. Hyman. 2005. Identification and characterization of factors required for microtubule growth and nucleation in the early *C. elegans* embryo. *Dev. Cell.* 9:223–236. doi:10.1016/j.devcel.2005.07.003

Srinivasan, D.G., R.M. Fisk, H. Xu, and S. van den Heuvel. 2003. A complex of LIN-5 and GPR proteins regulates G protein signaling and spindle function in *C. elegans*. *Genes Dev.* 17:1225–1239. doi:10.1101/gad.1081203

Tsou, M.-F.B., A. Hayashi, and L.S. Rose. 2003. LET-99 opposes Galpha/GPR signaling to generate asymmetry for spindle positioning in response to PAR and MES-1/SRC-1 signaling. *Development*. 130:5717–5730. doi:10.1242/dev.00790

van der Voet, M., C.W.H. Berends, A. Perreault, T. Nguyen-Ngoc, P. Gönczy, M. Vidal, M. Boxem, and S. van den Heuvel. 2009. NuMA-related LIN-5, ASPM-1, calmodulin and dynein promote meiotic spindle rotation independently of cortical LIN-5/GPR/Galpha. *Nat. Cell Biol.* 11:269–277. doi:10.1038/ncb1834